

Diphoton Signal of light pseudoscalar in NMSSM at the LHC

MONORANJAN GUHAIT ^{*} AND JACKY KUMAR [†]

*Department of High Energy Physics,
Tata Institute of Fundamental Research,
Homi Bhabha Road, Mumbai-400005, India*

November 7, 2018

Abstract

We explore the detection possibility of light pseudoscalar Higgs boson in the next-to-minimal supersymmetric Standard Model(NMSSM) at the LHC with the center of mass energy, $\sqrt{S} = 13$ TeV. We focus on the parameter space which provides one of the Higgs boson as the SM-like with a mass of 125 GeV and some of the non-SM-like Higgs bosons can be light having suppressed couplings with fermions and gauge bosons due to their singlet nature. It is observed that for certain region of model parameter space, the singlet like light pseudoscalar can decay to di-photon($\gamma\gamma$) channel with a substantial branching ratio. In this study, we consider this di-photon signal of light pseudoscalar Higgs boson producing it through the chargino-neutralino production and the subsequent decay of neutralino. We consider signal consisting of two photons plus missing energy along with a lepton from the chargino decay. Performing a detailed simulation of the signal and backgrounds including detector effects, we present results for a few benchmark points corresponding to the pseudoscalar Higgs boson mass in the range 60 -100 GeV. Our studies indicate that some of the benchmark points in the parameter space can be probed with a reasonable significance for 100 fb^{-1} integrated luminosity. We also conclude that exploiting this channel it is possible to distinguish the NMSSM from the other supersymmetric models.

^{*}guchait@tifr.res.in

[†]jka@tifr.res.in

1 Introduction

In spite of the absence of any signal of superpartners at the LHC, still supersymmetry(SUSY) remains one of the best possible option for the physics beyond standard model(BSM). Looking for its signal is a very high priority task in the next phase of LHC experiments. The SUSY models provide a solution for hierarchy problem, unify gauge couplings at a certain high energy scale and in addition, offers a dark matter candidate which is absent in the standard model(SM). In order to interpret the recently discovered Higgs particle(H_{SM}) of mass ~ 125 GeV at the LHC [1, 2] in the framework of the minimal supersymmetric standard model(MSSM), one requires a certain kind of parameter space, in particular for the squark sector of the third generation [3, 4]. For instance, the lightest Higgs boson of mass ~ 125 GeV in the MSSM can be obtained either by pushing up the lighter top squark mass to a larger value or assuming a maximal mixing in the top squark sector. Moreover, μ term in the superpotential, $\mu H_u H_d$ is a another potential source of problem, where H_u and H_d are the two Higgs doublets require to generate the up and down type of fermion masses. The value of μ is expected to be around the electroweak (EW) scale $\sim \mathcal{O}(100 \text{ GeV})$, but, nothing constrain it not to accept large value, in fact, it can go far above the EW scale, which is known as the μ -problem [5]. In the framework of the Next-to-minimal supersymmetric model (NMSSM) these issues can be addressed more naturally [6–8]. The NMSSM contains an extra Higgs singlet field(S), in addition to the two Higgs doublets H_u, H_d like the MSSM and, the superpotential reads as,

$$W_{\text{NMSSM}} = W_{\text{MSSM}} + \lambda S H_u H_d + \frac{1}{3} \kappa S^3, \quad (1.1)$$

where λ and κ are the dimensionless couplings and W_{MSSM} is the part of the superpotential in the MSSM, except the μ term. After the electroweak symmetry breaking, the vacuum expectation value(VEV) of the singlet field (S) v_s , generates the μ term dynamically, i.e $\mu_{\text{eff}} = \lambda v_s$. The Higgs sector of the NMSSM contains three neutral CP even(H_1, H_2, H_3 ; $m_{H_1} < m_{H_2} < m_{H_3}$) and two CP odd neutral pseudoscalars(A_1, A_2 ; $m_{A_1} < m_{A_2}$) plus charged Higgs boson (H^\pm) states (for details, see the review of Ref. [9] and Ref. [10]). The states of the physical neutral Higgs bosons are composed of both the singlet and the doublet fields. Interestingly, one of the CP even neutral Higgs boson can be interpreted as the recently found SM-like Higgs boson and it remains valid for a wide range of model parameters [11–16] and, unlike the MSSM, it does not require much fine tuning of the model parameters. It can be attributed to the mixing of the singlet Higgs field with the doublets via $\lambda S H_u H_d$ term. As a consequence, this interaction, in turn lifts the tree level Higgs boson mass substantially and then further contribution

due to the radiative correction enable to achieve the required Higgs boson mass of ~ 125 GeV [15, 16]. Naturally, with the discovery of the Higgs boson [1, 2], the NMSSM has drawn a lot attention, in general, to study in more details the Higgs sector and the corresponding phenomenology at the LHC with a great interest [12–14, 17–20]. Previous studies showed that in the NMSSM framework, the scenario of very light Higgs bosons (<125 GeV) exist, while one of the CP even neutral Higgs boson SM like [13, 14, 21–24]. Notably, these light Higgs bosons are non-SM like and dominantly singlet in nature and, hence not excluded by any past experiments due to the suppression of their production in colliders. Needless to say, in the present context of continuing Higgs studies in the LHC experiments, it is one of the priority to search for these light non SM-like Higgs bosons.

Already, in Run 1 experiments at the LHC, extensive searches were carried out for the lightest CP odd Higgs boson(A_1) either producing it directly or via the decay of the SM-like Higgs boson, $H_{\text{SM}} \rightarrow A_1 A_1$. The CMS experiment performed searches through direct production of A_1 and decaying to a pair of muons [25] and taus [26] for the mass ranges 5.5 - 14 GeV and 25-80 GeV respectively and, also looked for it in the SM Higgs decay in 4τ final states [26]. The ATLAS collaboration published results for A_1 searches, $H_{\text{SM}} \rightarrow A_1 A_1 \rightarrow \mu\mu\tau\tau$ decays with a mass range 3.7 - 50 GeV [27] and also in four photon final states corresponding to the mass range 10 - 62 GeV [28]. From the non observation of any signal in all those searches, the exclusion of cross sections folded with branching ratios(BR) for a given channel are presented for the mass range $\sim 5 - 60$ of A_1 .

On the phenomenological side, after the discovery of the Higgs boson at the LHC, detection prospects of all Higgs bosons in the NMSSM are revisited [29–31]. Nonetheless, it is more appealing to explore the detection possibility of the light non SM-like Higgs bosons in various interesting decay channels to establish the NMSSM effects which are absent in the MSSM. In this context, searching for lighter Higgs bosons, in particular A_1 is very interesting, since it can be very light [32, 33]. There are many phenomenological analysis reported in the literature exploring the detection prospect of A_1 at the LHC [34–39]. In our study as reported in [21], the rates of production of non SM-like Higgs bosons in various decay channels are estimated for the LHC Run 2 experiment with the center of mass energy, $\sqrt{S}=13$ TeV. Remarkably, it is observed that along with the dominant $b\bar{b}$ and $\tau\tau$ decay modes of non SM-like Higgs bosons, the BR for two photon ($\gamma\gamma$) decay mode is also very large for a certain part of the parameter space. In particular, light A_1 decays to $\gamma\gamma$ mode with a BR ranging from a few percent to 80-90% for a substantial region of the parameter space [19, 21, 39–43]. On the other side, as we know, experimentally photon is a very clean object and can

schematically it is presented in Fig. 1. The final state contains hard missing energy due to the presence of neutrinos and neutralinos($\tilde{\chi}_1^0$) which are assumed to be the lightest SUSY particle(LSP) and stable¹, and escape the detector, since they are weakly interacting. Finally, the reaction,Eq. 1.2 leads to the signal,

$$\gamma\gamma + \ell^\pm + \cancel{E}_T. \quad (1.3)$$

Of course, in addition to the chargino-neutralino production cross section, the $\text{BR}(\tilde{\chi}_{2,3}^0 \rightarrow \tilde{\chi}_1^0 A_1)$ and $\text{BR}(A_1 \rightarrow \gamma\gamma)$, which are sensitive to the parameter space, very crucial in determining the signal rate. In view of this, we investigate the sensitivity of this signal to the relevant parameters scanning those systematically for a wide range and identify the suitable region which provides the reasonable rate of the signal. Finally, out of this parameter scan, we select few benchmark parameter points for which results are presented. Performing a detail simulation including detector effects for both the signal and the SM backgrounds processes, we predict the signal significances corresponding to our choices of parameters for a few integrated luminosity options at the LHC with the center of mass energy, $\sqrt{S}=13$ TeV.

This paper is organized as follows, In section 2, after briefly discussing the chargino and neutralino sector in the NMSSM, we study the parameter space sensitivity of chargino-neutralino associated production cross section. The parameter sensitivity of BRs of neutralinos and A_1 decays are discussed in section 3 and then propose few benchmark points for which results are presented. The details of the simulation are presented in section 4, while results are discussed in section 5. Finally, we summarize in section 6.

2 Chargino-Neutralino production

The chargino-neutralino associated production($\tilde{\chi}_1^\pm \tilde{\chi}_{2,3}^0$) in proton-proton collision is mediated purely by electro-weak(EW) interaction at the tree level and, hence very sensitive to the parameters space owing to the dependence of couplings. Therefore, in order to understand the various features of this production process at the LHC, it is worth to discuss the interplay between parameters and cross sections.

2.1 Chargino and Neutralino sector in NMSSM

In SUSY model, there are spin half EW gauginos and Higgsinos which are the supersymmetric partners of the gauge bosons and Higgs bosons respectively. The soft

¹We are considering R-Parity conserving model.

mass terms for gauginos and the spontaneous breaking of EW symmetry lead a mixing between gaugino and Higgsino states making them weak eigenstates without physical mass terms. The charginos are the mass eigenstates corresponding to the mixed charged gaugino and Higgsino states. Similarly, the mixings of neutral EW gauginos and Higgsinos produce physical neutralinos. The masses and the corresponding physical states can be obtained by diagonalizing the respective mass matrices. For instance, the masses of the chargino states ($\tilde{\chi}_{1,2}^\pm$) are obtained diagonalizing the 2×2 chargino mass matrix by a bi-unitary transformation. In the MSSM, the masses and composition of these chargino states are determined by M_2 - the $SU(2)$ gaugino mass parameter, μ and $\tan\beta$ - the ratio of two vacuum expectation values (v_u, v_d) of the neutral components of two Higgs doublets require to break EW symmetry spontaneously. In the NMSSM, the presence of an extra Higgs singlet field does not modify the chargino sector, hence it remains same as in the MSSM, except the Higgsino mass parameter μ which is replaced by μ_{eff} .

On contrary, in the NMSSM, the neutralino sector is extended due to the addition of an extra singlino state \tilde{S} - the fermionic superpartner of the singlet scalar field (S). Here \tilde{S} mixes with the Higgsinos due to the presence of the $\lambda H_u H_d S$ term in the superpotential. Thus, the resulting 5×5 neutralino mass matrix is given by,

$$M_N = \begin{pmatrix} M_1 & 0 & \frac{-g_1 v c_\beta}{\sqrt{2}} & \frac{g_1 v s_\beta}{\sqrt{2}} & 0 \\ 0 & M_2 & \frac{g_2 v c_\beta}{\sqrt{2}} & \frac{-g_2 v s_\beta}{\sqrt{2}} & 0 \\ \frac{-g_1 v c_\beta}{\sqrt{2}} & \frac{g_2 v c_\beta}{\sqrt{2}} & 0 & -\mu_{\text{eff}} & -\lambda v s_\beta \\ \frac{g_1 v s_\beta}{\sqrt{2}} & \frac{-g_2 v s_\beta}{\sqrt{2}} & -\mu_{\text{eff}} & 0 & -\lambda v c_\beta \\ 0 & 0 & -\lambda v s_\beta & -\lambda v c_\beta & 2\kappa v_s \end{pmatrix}. \quad (2.1)$$

Here M_1 is the mass of $U(1)$ gaugino - the bino(\tilde{B}) and g_1, g_2 are the weak gauge couplings. In the MSSM limit, *i.e.* $\lambda, \kappa \rightarrow 0$, this 5×5 neutralino mass matrix reduces to a 4×4 mass matrix. The masses of neutralinos can be derived by diagonalizing symmetric matrix M_N via a unitary transformation as,

$$M_{\tilde{\chi}^0}^D = N M_N N^\dagger. \quad (2.2)$$

with N as a unitary matrix. The analytical solution of the neutralino mass matrix presenting the spectrum of neutralino masses and mixings exist in the literature for the MSSM [47, 48]. However for the NMSSM, the 5th order eigenvalue equation makes it more difficult to extract exact analytical solution. Nevertheless, attempts are there to find the approximate analytical solution [49, 50]. Consequently, the five physical neutralino states become the admixtures of weak states, such as gauginos, Higgsinos

and singlino. Hence, in the basis $\tilde{\psi}^0 \equiv (-i\tilde{B}, -i\tilde{W}_3, \tilde{H}_d^0, \tilde{H}_u^0, \tilde{S})$, the physical neutralino states are composed of,

$$\tilde{\chi}_i^0 = N_{ij}\tilde{\psi}_j^0, \quad (2.3)$$

where $N_{ij}(i,j=1-5)$ is defined by Eq. 2.2. In particular, N_{i5} presents the singlino component in the i -th physical neutralino state. To conclude, in the NMSSM, the masses and the mixings of the charginos and neutralinos at the tree level can be determined by 6 parameters, namely,

$$M_1, \quad M_2, \quad \tan \beta, \quad \mu_{eff}, \quad \lambda, \quad \kappa. \quad (2.4)$$

Here one can choose M_1 and M_2 to be real and positive by absorbing phases in \tilde{B}^0 and \tilde{W}^0 respectively, but in general μ_{eff} can be complex. In this current study, we assume CP-conserving NMSSM setting all the input parameters real.

A careful examination of the neutralino mass matrix reveals few characteristic features of this sector [49,50]. For instance, notice that the singlet field does not mix with the gauge fields, and hence the singlino like neutralino states do not interact with the gaugino like states or gauge fields. Apparently, two out of the five neutralino states remain to be gaugino like if, $|M_{1,2} - \mu_{eff}| > M_Z$. Note that the direct singlet-doublet mixing is determined by λ . The mass of the singlino like neutralino is given by $|2\kappa v_s|$, and so if $|2\kappa v_s| \ll M_{1,2}, \mu_{eff}$, then the lighter neutralino state becomes dominantly a singlino like. On the other hand, if $|2\kappa v_s| \gg M_{1,2}, \mu_{eff}$, then the singlino state completely decouples from the other states resulting all four neutralino states mixtures of gaugino-Higgsino, *i.e* a MSSM like scenario, where as the remaining heavier neutralino state appears to be completely singlino like. The coupling structures of neutralinos with gauge bosons and fermions remain the same as in the MSSM, since the singlet field does not interact with them. For the sake of discussion in the later section, we present the $\tilde{\chi}_1^\pm - \tilde{\chi}_j^0 - W^\mp$ interaction,

$$g_{\tilde{\chi}_1^\pm \tilde{\chi}_j^0 W^\mp}^L = \frac{e}{s_w} \left(N_{j2} V_{11}^* - \frac{1}{\sqrt{2}} N_{j4} V_{12}^* \right), \quad g_{\tilde{\chi}_1^\pm \tilde{\chi}_j^0 W^\mp}^R = \frac{e}{s_w} \left(N_{j2}^* U_{11} + \frac{1}{\sqrt{2}} N_{j3}^* U_{12} \right), \quad (2.5)$$

and $q - \tilde{q} - \tilde{\chi}_j^0$ couplings,

$$g_{d\tilde{d}\tilde{\chi}_j^0}^L \approx \frac{-e}{\sqrt{2}s_w c_w} \left(\frac{1}{3} N_{j1} s_w - N_{j2} c_w \right), \quad g_{d\tilde{d}\tilde{\chi}_j^0}^R \approx 0, \quad (2.6)$$

$$g_{u\tilde{u}\tilde{\chi}_j^0}^L \approx \frac{-e}{\sqrt{2}s_w c_w} \left(\frac{1}{3} N_{j1} s_w + N_{j2} c_w \right), \quad g_{u\tilde{u}\tilde{\chi}_j^0}^R \approx 0. \quad (2.7)$$

with $s_w = \sin \theta_w, c_w = \cos \theta_w$ and $j=2,3$. Note that, since we consider only the first two generations of squarks and assume that the chiral mixings are negligible, hence we

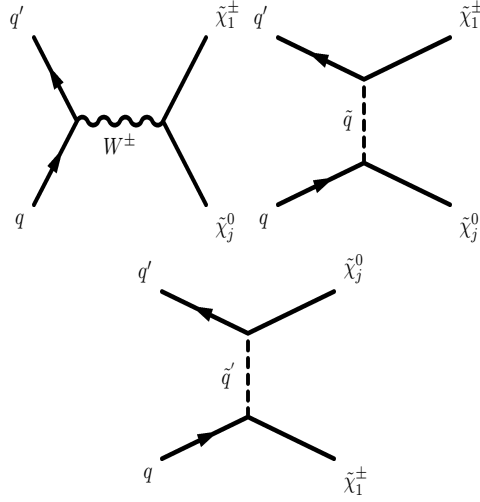


Figure 2: Tree level Feynman diagrams for chargino-neutralino associated production via q and \bar{q} annihilation.

omit the corresponding interaction terms and, for the same reasons, $g_{u\bar{u}\tilde{\chi}_j^0}^R$ and $g_{d\bar{d}\tilde{\chi}_j^0}^R$ are negligible. Apparently, the presence of the direct effect of NMSSM through singlino component is absent in these interactions. However, because of the unitarity of the mixing matrix N , the singlino component N_{i5} indirectly affects these couplings. It will be discussed more in the next sub-section in the context of the chargino-neutralino production.

2.2 $\tilde{\chi}_1^\pm \tilde{\chi}_j^0$ cross-section

In this section, in the framework of the NMSSM, we discuss various features of the chargino-neutralino ($\tilde{\chi}_1^\pm \tilde{\chi}_j^0, j=1,2,3$) associated production at the LHC. For the sake of comparison and discussion, we also study $\tilde{\chi}_1^\pm \tilde{\chi}_1^0$ production cross section, although it has no relevance to our present context. As already mentioned, in hadron colliders, the chargino-neutralino pairs are produced purely via EW interaction initiated by quark and anti-quark annihilation as,

$$q\bar{q}' \rightarrow \tilde{\chi}_1^\pm \tilde{\chi}_j^0; \quad j = 1, 2, 3, \quad (2.8)$$

the corresponding Feynman diagrams at the tree level are shown in Fig. 2. The s and t/u -channels are mediated by the W boson and the first two generations of squarks respectively and, are very sensitive to the couplings, see Eq. 2.5–2.7, which are regulated by model parameters. In case, if both the chargino and the neutralino states be pure Higgsino like, then the t and u channel diagrams decouple completely due to the

suppressed quark-squark-neutralino couplings(Eqs. 2.6, 2.7), otherwise mixed or pure gaugino like states are favored. The contribution of the t/u -channel diagrams are also suppressed for heavier masses of squarks. Moreover, negative interference of the s and t/u channel diagrams yields an enhancement of the production cross section for heavier masses of squarks for a given set of other parameters.

The partonic level differential $\tilde{\chi}_1^\pm \tilde{\chi}_j^0$ cross section in NMSSM can be obtained following the form given in Ref. [51] for the MSSM,

$$\begin{aligned} \frac{d\hat{\sigma}(q\bar{q} \rightarrow \tilde{\chi}_i^\pm \tilde{\chi}_j^0)}{d\hat{t}} &= \frac{\pi\alpha^2}{3\hat{s}^2} [|Q_{LL}|^2 (\hat{u} - m_{\tilde{\chi}_j^0}^2) (\hat{u} - m_{\tilde{\chi}_i^\pm}^2) + |Q_{LR}|^2 (\hat{t} - m_{\tilde{\chi}_j^0}^2) (\hat{t} - m_{\tilde{\chi}_i^\pm}^2) \\ &\quad + 2 \hat{s} \operatorname{Re}(Q_{LL}^* Q_{LR}) m_{\tilde{\chi}_j^0} m_{\tilde{\chi}_i^\pm}] \end{aligned} \quad (2.9)$$

which is expressed in terms of four helicity charges $Q_{LL}, Q_{LR}, Q_{RL}, Q_{RR}$. For the sake of completeness, we also present the explicit form of these charges [51],

$$\begin{aligned} Q_{LL} &= \frac{1}{\sqrt{2}s_w^2} \left[\frac{N_{j2}^* V_{i1} - 1/\sqrt{2} N_{j4}^* V_{i2}}{\hat{s} - M_W^2} + V_{i1} \frac{I_{3\tilde{q}} N_{j2}^* + (e_{\tilde{q}} - I_{3\tilde{q}}) N_{j1}^* \tan \theta_w}{\hat{u} - m_{\tilde{q}}^2} \right], \\ Q_{LR} &= \frac{1}{\sqrt{2}s_w^2} \left[\frac{N_{j2} U_{i1}^* + 1/\sqrt{2} N_{j3} U_{i2}^*}{\hat{s} - M_W^2} - (U_{i1})^* \frac{I_{3\tilde{q}'} N_{j2} + (e_{\tilde{q}'} - I_{3\tilde{q}'}) N_{j1} \tan \theta_w}{\hat{t} - m_{\tilde{q}'}^2} \right], \\ Q_{RR} &= Q_{RL} = 0, \end{aligned} \quad (2.10)$$

where the Mandelstam variables are defined as, $\hat{s} = (p_1 + p_2)^2$; $\hat{t} = (p_1 - p_3)^2$; $\hat{u} = (p_2 - p_4)^2$ in the partonic frame, p_1, p_2 are the momenta of initial quarks, p_3, p_4 represent the same for $\tilde{\chi}_i^\pm$ and $\tilde{\chi}_j^0$ respectively. Notice that, as pointed out earlier, even without any explicit dependence of couplings, Eqs. 2.5, 2.6 and 2.7, on the singlino composition, N_{j5} in the neutralino state, nonetheless, it affects the $\tilde{\chi}_1^\pm \tilde{\chi}_j^0$ production cross section due to the dilution of gaugino and Higgsino components.

We compute this leading order(LO) cross section setting QCD scales, $Q^2 = \hat{s}$ -the partonic center of mass energy and for the choice of CT10 [52] parton distribution function. The corresponding next to leading order(NLO) predictions for the $\tilde{\chi}_1^\pm \tilde{\chi}_j^0$ cross sections are obtained from Prospino [53] and the k-factor($=\sigma_{\text{NLO}}/\sigma_{\text{LO}}$) is found to be ~ 1.3 [51]. In the present NMSSM case, to take care NLO effects in the cross-section, we use the same k-factor, which is not expected to be too different with respect to the MSSM case. We observe that LO chargino-neutralino associated production cross-section varies from sub femto-barn(fb) level to to few pico-barn(pb) for the mass range of 100-500 GeV of charginos and neutralinos.

To understand the dependence of $\tilde{\chi}_1^\pm \tilde{\chi}_j^0$ cross sections on the parameters, we demonstrate its variation in Fig. 3 and Fig. 4, primarily for gaugino and Higgsino like

scenarios varying M_2 and μ_{eff} respectively. The variation of singlino composition are controlled by a set of few choices of $\lambda, \kappa = [a] 0.1, 0.7, [b] 0.2, 0.1$ for Fig. 3 and $\lambda, \kappa = [a] 0.7, 0.1, [b] 0.2, 0.1$ and $[c] 0.4, 0.1$ for Fig. 4. The other parameters are set as, $\tan \beta = 10$, $\mu_{\text{eff}} = 1000$ GeV (for Fig. 3), $M_2 = 600$ GeV (for Fig. 4), squark masses $m_{Q_L}, m_{D_{L,R}} = 1000$ GeV and assuming the relation $M_1 = M_2/2$. In the following, we discuss the variation of cross sections with the sensitive parameters which has some impact on the signal sensitivity, as will be discussed in the later sections.

- The dependence of $\tilde{\chi}_1^\pm \tilde{\chi}_j^0$ cross section on M_2 , in the gaugino like scenario ($M_2 < \mu_{\text{eff}} = 1000$ GeV) is presented in Fig. 3. In this scenario, in the case of $\lambda, \kappa = [a] 0.1, 0.7$, the mass of singlino is very heavy ($\sim |2\kappa v_s| = 2\mu_{\text{eff}}\kappa/\lambda = 14$ TeV) and the $\tilde{\chi}_1^\pm$ state is wino like of mass around M_2 , while the $\tilde{\chi}_1^0$ is bino dominated with its mass about $m_{\tilde{\chi}_1^0} \sim M_1$. On the other hand, because of large mass of the singlino state and lower value of λ , *i.e.* small singlet-doublet mixing, the $\tilde{\chi}_2^0$ and $\tilde{\chi}_3^0$ states are turn out to be dominantly wino and Higgsino like respectively, with masses $m_{\tilde{\chi}_2^0} \sim M_2$ and $m_{\tilde{\chi}_3^0} \sim \mu_{\text{eff}}$. It explains the reasons of larger $\tilde{\chi}_1^\pm \tilde{\chi}_2^0$ cross section in comparison to $\tilde{\chi}_1^\pm \tilde{\chi}_1^0$, as seen in Fig. 3[a]. Note that, the subsequent fall of both the cross sections with the increase of M_2 is purely a mass effect. Obviously, the $\tilde{\chi}_1^\pm \tilde{\chi}_3^0$ cross section is expected to be suppressed and almost negligible dependence on M_2 . However, in the case of $\lambda, \kappa = [b] 0.7, 0.1$, the singlino state becomes comparatively light with mass about ~ 300 GeV. In this scenario, due to the large singlet-doublet mixing ($\lambda = 0.7$), at the lower values of M_2 , the $\tilde{\chi}_3^0$ state is found to be singlino like with very less wino and Higgsino components, whereas $\tilde{\chi}_2^0, \tilde{\chi}_1^0$ states appear to be more or less wino and bino like respectively. Consequently, in this lower region of M_2 , the $\tilde{\chi}_1^\pm \tilde{\chi}_{1,2}^0$ cross sections are higher than the $\tilde{\chi}_1^\pm \tilde{\chi}_3^0$, mainly due to the suppressed couplings of $\tilde{\chi}_3^0$ with gauge boson and fermions being it a dominantly a singlino state. However, with the increase of M_2 , the wino (singlino) component in $\tilde{\chi}_2^0$ ($\tilde{\chi}_3^0$) decreases, resulting a gradual fall (enhancement) of $\tilde{\chi}_1^\pm \tilde{\chi}_2^0$ ($\tilde{\chi}_1^\pm \tilde{\chi}_3^0$) cross sections. Eventually, as M_2 reaches closer to $|2\kappa v_s| \sim 300$ GeV, the $\tilde{\chi}_2^0$ and $\tilde{\chi}_3^0$ states tend to be singlino and wino like respectively and, hence due to the depletion of $\tilde{\chi}_1^\pm \tilde{\chi}_2^0$ cross section very sharply, $\tilde{\chi}_1^\pm \tilde{\chi}_3^0$ cross section takes over it and then falls slowly mainly due to the phase space suppression, see Fig. 3[b]. However, in contrast, due to the larger mass of singlino (~ 14 TeV) the similar type of crossing between $\tilde{\chi}_1^\pm \tilde{\chi}_2^0$ and $\tilde{\chi}_1^\pm \tilde{\chi}_3^0$ cross sections is not observed in Fig. 3[a].

- The variation of cross sections with μ_{eff} , for Higgsino like scenario is presented in Fig. 4, keeping $M_2 = 600$ GeV and for three combinations of $\lambda, \kappa = [a] 0.1, 0.7, [b] 0.2, 0.1, [c] 0.4, 0.1$. In this scenario, the $\tilde{\chi}_1^\pm$ state is mostly Higgsino like for the lower range of μ_{eff} , and then becomes a gaugino-Higgsino mixed state when $\mu_{\text{eff}} \sim M_2$. For the scenario [a], at the lower range of $\mu_{\text{eff}} (\lesssim M_1 = 300$ GeV), the Higgsino composition

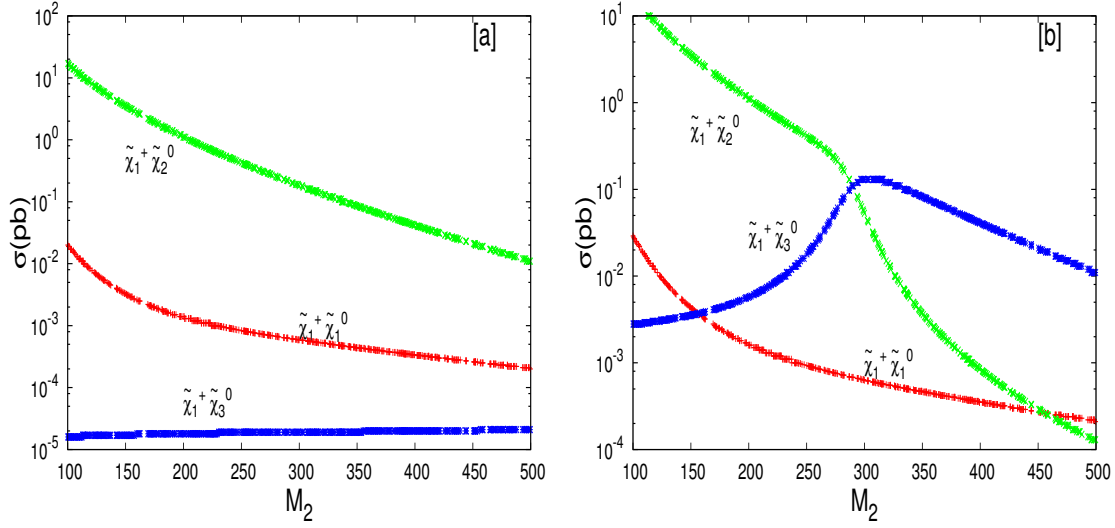


Figure 3: Variation of leading order (LO) chargino-neutralino associated production cross section with M_2 , at the LHC energy $\sqrt{S} = 13$ TeV and for two choices of λ, κ =[a] 0.1,0.7, [b] 0.7,0.1. The other parameters are set as, $\mu_{\text{eff}} = 1000$ GeV, $M_1 = M_2/2$, $\tan \beta = 10$.

in $\tilde{\chi}_1^0$ state is the dominant one, but it becomes bino like once $\mu_{\text{eff}} \gtrsim M_1$ and a drop of $\tilde{\chi}_1^\pm \tilde{\chi}_1^0$ cross section occurs beyond $\mu_{\text{eff}} \sim 300$ GeV, as seen in Fig. 4[a]. However, for the scenario, [b] and [c], at the lower side of μ_{eff} , the $\tilde{\chi}_1^0$ state, along with some Higgsino component, contains a finite fraction of singlino (recall the singlino mass $\sim 2\mu_{\text{eff}}\kappa/\lambda$), and in particular, for the scenario[c], $\tilde{\chi}_1^0$ becomes dominantly a singlino like. Nevertheless, the $\tilde{\chi}_1^\pm \tilde{\chi}_1^0$ cross section are not heavily suppressed due to the presence of mild Higgsino component in the $\tilde{\chi}_1^0$ state. The Higgsino and bino like nature of $\tilde{\chi}_2^0$ yields a steady variation of $\tilde{\chi}_1^\pm \tilde{\chi}_2^0$ cross section with μ_{eff} , except for the case [b] where a sudden drop and then further an enhancement is observed at $\mu_{\text{eff}} \sim 300$ GeV. Here both the singlino and the bino masses are around ~ 300 GeV, implying an increase of singlino and bino components in $\tilde{\chi}_2^0$ state causing a drop of $\tilde{\chi}_1^\pm \tilde{\chi}_2^0$ cross section and beyond this region, again it goes up with the increase of μ_{eff} due to further increase of its Higgsino component. In the presence of small singlet-doublet mixings, in the scenario λ, κ =[a] 0.1,0.7, the $\tilde{\chi}_3^0$ state is bino dominated at the lower range of $\mu_{\text{eff}} < M_1$, resulting comparatively a lower $\tilde{\chi}_1^\pm \tilde{\chi}_3^0$ cross section, which slowly increases with μ_{eff} due to the enhancement of Higgsino composition in it, as observed in Fig.4[a]. In Fig.4[b], it is found that the singlino composition in $\tilde{\chi}_3^0$ state goes up with the increase of μ_{eff} , while it is below $|2\kappa v_s|$ and, becomes completely singlino like at $\mu_{\text{eff}} \sim |2\kappa v_s|$ (~ 300 GeV) hence the rapid fall of $\tilde{\chi}_1^\pm \tilde{\chi}_3^0$ cross section. Beyond $\mu_{\text{eff}} > |2\kappa v_s|$ region, Higgsino composition in the $\tilde{\chi}_3^0$ state increases yielding more higher $\tilde{\chi}_1^\pm \tilde{\chi}_3^0$ cross section and then due to mass effect, it falls slowly.

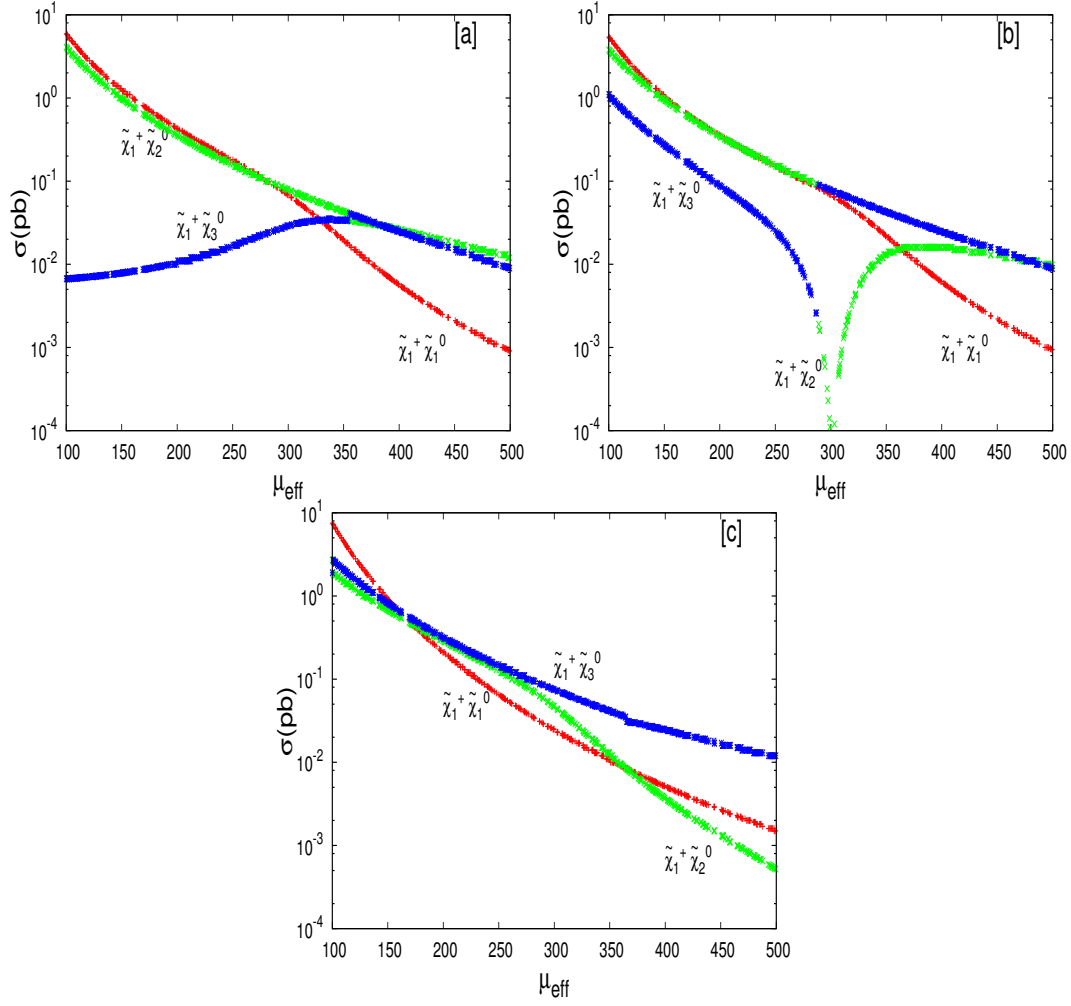


Figure 4: Variation of LO chargino-neutralino associated production cross section with μ_{eff} , at the LHC energy $\sqrt{S}=13$ TeV and for the choices of $\lambda, \kappa=[a] 0.1, 0.7$, [b] $0.2, 0.1$, [c] $0.4, 0.1$. The other parameters are set as, $M_2=600$ GeV, $M_1 = M_2/2$, $\tan \beta = 10$.

3 Decays : $\tilde{\chi}_{2,3}^0 \rightarrow \tilde{\chi}_1^0 A_1$; $A_1 \rightarrow \gamma\gamma$

As stated earlier, the sensitivity of the signal $\ell + \gamma\gamma + \cancel{E}_T$, crucially depends on the combined effects of the $\tilde{\chi}_1^\pm \tilde{\chi}_{2,3}^0$ production cross section and subsequent BRs involved in the cascade decays, such as $\tilde{\chi}_{2,3}^0 \rightarrow \tilde{\chi}_1^0 A_1$ and $A_1 \rightarrow \gamma\gamma$, $\tilde{\chi}_1^\pm \rightarrow \tilde{\chi}_1^0 \ell \nu$. Note that the $\text{BR}(\tilde{\chi}_1^\pm \rightarrow \tilde{\chi}_1^0 \ell^\pm \nu)$ is almost the same as the leptonic BR of W-boson for our considered parameter space.

In this section, the sensitivity of the signal, Eq. 1.3 cross sections with the parameters are studied systematically by scanning those using **NMSSMTools4.9.0** [54] taking into account various constraints such as dark matter, flavor physics and direct searches

at LEP and LHC experiments. In this numerical scan we use the following range of parameters:

$$\begin{aligned}
0.1 < \lambda < 0.7; \quad 0.1 < \kappa < 0.7; \quad 0 < A_\lambda < 2 \text{ TeV}, \quad -9 < A_\kappa < -4 \text{ GeV}; \\
2 < \tan \beta < 50; \quad 140 \text{ GeV} < \mu_{\text{eff}} < 600 \text{ GeV} \\
M_{Q_3} = M_{U_3} = 1 - 3 \text{ TeV}, \quad A_t = -3 - (+3) \text{ TeV},
\end{aligned} \tag{3.1}$$

The other soft masses are set as

$$\begin{aligned}
M_{Q_{1/2}} = M_{U_{1/2}} = M_{D_{1/2}} = M_{D_3} = M_{L_3} = M_{E_3} = A_{E_3} = 1 \text{ TeV} \\
A_b = 2 \text{ TeV}, M_{L_{1,2}} = M_{E_{1,2}} = 200 \text{ GeV}, A_{E_{1,2}} = 0.
\end{aligned}$$

The important factors in this discussion are the mass and the composition of A_1 which is dominantly a singlet like. In order to understand the variation of composition of A_1 , here we briefly revisit the Higgs mass matrix corresponding to CP-odd states. The initial 3×3 CP odd Higgs mass matrix reduces to 2×2 matrix after rotating away the Goldstone mode. Hence, the CP-odd mass matrix, M_P^2 , in the basis of doublet(A) and singlet(S), is given by [9, 10],

$$M_P^2 = \begin{pmatrix} M_A^2 & \lambda(A_\lambda - 2\kappa v_s)v \\ \lambda(A_\lambda - 2\kappa v_s)v & M_S^2 \end{pmatrix}, \tag{3.2}$$

where

$$M_A^2 = \frac{2\mu_{\text{eff}}(A_\lambda + \kappa v_s)}{\sin 2\beta}, \quad M_S^2 = \lambda(A_\lambda + 4\kappa v_s) \frac{v_u v_d}{v_s} - 3\kappa A_\kappa v_s. \tag{3.3}$$

This 2×2 mass matrix can be diagonalized by an orthogonal rotation with an angle α , as given by,

$$\tan 2\alpha = \frac{2M_{12}^2}{(M_A^2 - M_S^2)}, \tag{3.4}$$

where $M_{12}^2 = \lambda(A_\lambda - 2\kappa v_s)v$ and $v = \sqrt{v_u^2 + v_d^2}$. Obviously, two mass eigenstates (A_1, A_2) are the mixtures of the doublet (A) and the singlet (S) weak eigen states.

• $\tilde{\chi}_j^0 \rightarrow \tilde{\chi}_1^0 A_1$, $j=2,3$: The relevant part of the coupling (Higgsino-Higgsino-Singlet) for this decay channel is given by,

$$g_{\tilde{\chi}_j^0 \tilde{\chi}_1^0 A_1} \approx \frac{i}{\sqrt{2}} \lambda P_{13} (N_{j4} N_{13} + N_{j3} N_{14}). \tag{3.5}$$

Here $P_{13} \sim \cos \alpha$ presents the singlino composition in A_1 . Hence, for very small values of $\sin \alpha$ this coupling favors only the Higgsino like $\tilde{\chi}_j^0$ and $\tilde{\chi}_1^0$ states. Note that, in the

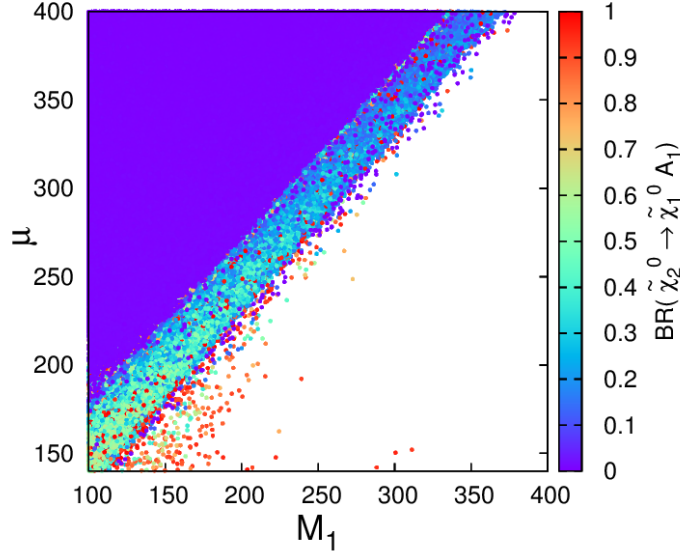


Figure 5: $\text{BR}(\tilde{\chi}_2^0 \rightarrow \tilde{\chi}_1^0 A_1)$ in the $M_1 - \mu_{eff}$ plane. All energy units are in GeV.

context of our signal, the gaugino like $\tilde{\chi}_j^0$ and $\tilde{\chi}_1^0$ states are not favoured in order to suppress the decay modes such as, $\tilde{\chi}_j^0 \rightarrow \tilde{\chi}_1^0 Z, \ell\bar{\ell}$. This type of Higgsino like scenario can be achieved by setting $\mu_{eff} \sim M_1 < M_2$, which also makes $\tilde{\chi}_{2,3}^0$ and $\tilde{\chi}_1^0$ states almost degenerate, i.e $m_{\tilde{\chi}_2^0} \sim m_{\tilde{\chi}_1^0}$, a compressed like scenario. However, in order to have a reasonable sensitivity of this signal, the visible decay spectrum are expected to be little bit harder to pass kinematic thresholds, which can be ensured by setting the mass splitting, $\Delta m = m_{\tilde{\chi}_{2,3}^0} - m_{\tilde{\chi}_1^0}$ to a reasonable value. This requirement leads us to choose M_1 less than μ_{eff} , but of course, not by a huge gap to retain sufficient Higgsino component, making $\tilde{\chi}_1^0$ a bino-Higgsino mixed state. In Fig.5, we show the correlation of $\text{BR}(\tilde{\chi}_2^0 \rightarrow \tilde{\chi}_1^0 A_1)$ in the $M_1 - \mu_{eff}$ plane. Notice that the 10% or more $\text{BR}(\tilde{\chi}_2^0 \rightarrow \tilde{\chi}_1^0 A_1)$ corresponds to the region $M_1 \sim \mu_{eff}$ and, we found that it remains to be valid for a wide range of λ and κ . This figure clearly reflects the preferred choices of M_1 and μ_{eff} for our considered signal channel.

- $A_1 \rightarrow \gamma\gamma$: The earlier studies [19,21,40,41] showed that the variation of BR of non SM-like NMSSM Higgs bosons in various decay channels is very dramatic depending on the region of parameters. For instance, the singlet like A_1 state decouples from the fermions leading a suppression of the tree level decay modes $b\bar{b}$ and $\tau\tau$ and an enhancement of $\text{BR}(A_1 \rightarrow \gamma\gamma)$ channel [19,40,41]. The cause of having a finite partial $A_1 \rightarrow \gamma\gamma$ decay width can be understood by examining the respective coupling structures of A_1 with two photons [55]. The A_1 state decays to two photons via loops comprising heavy fermions and charginos [56,57], see Fig.6. The partial decay width

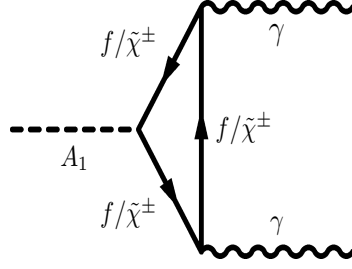


Figure 6: Loop diagrams for the decay of A_1 to two photons, mediated by fermion (f) and chargino($\tilde{\chi}^\pm$).

of $A_1 \rightarrow \gamma\gamma$ can be obtained simply using the MSSM expression, but replacing the respective couplings to the NMSSM values. Thus, it is given as [56, 57],

$$\Gamma(A_1 \rightarrow \gamma\gamma) = \frac{G_F \alpha_{em}^2 M_{A_1}^3}{32\sqrt{2}\pi^3} \left| \sum_f N_c e_f^2 g_f^{A_1} A_f(\tau_f) + \sum_{\tilde{\chi}_i^\pm} g_{\tilde{\chi}_i^\pm}^{A_1} A_{\tilde{\chi}_i^\pm}(\tau_{\tilde{\chi}_i^\pm}) \right|^2. \quad (3.6)$$

Here N_c is the QCD color factor, e_f is the electric charge of the fermions (f), $A_x(\tau_x)$ are the loop functions given by,

$$A_x(\tau_x) = \tau_x \left(\sin^{-1} \frac{1}{\sqrt{\tau_x}} \right)^2, \quad \tau_x = \frac{4M_x^2}{M_{A_1}^2}; \quad x = f, \tilde{\chi}_i^\pm. \quad (3.7)$$

Here $g_f^{A_1}$ are the couplings of A_1 with the heavier fermions (f =top and bottom quarks), where as $g_{\tilde{\chi}^\pm}^{A_1}$ are the same with charginos, and all those are given by [9],

$$g_u^{A_1} = -i \frac{m_u}{\sqrt{2}v \sin \beta} P_{12}, \quad g_d^{A_1} = i \frac{m_d}{\sqrt{2}v \cos \beta} P_{11}, \quad (3.8)$$

$$g_{\tilde{\chi}_i^\pm \tilde{\chi}_j^\mp A_1} = \frac{i}{\sqrt{2}} [\lambda P_{13} U_{i2} V_{j2} - g_2 (P_{12} U_{i1} V_{j2} + P_{11} U_{i2} V_{j1})] \quad (3.9)$$

Here P and (U, V) are the mixing matrices for pseudoscalar Higgs bosons and chargino sector respectively and, in particular $P_{11} = \sin \alpha \sin \beta$ and $P_{12} = \sin \alpha \cos \beta$. In the pure singlet limit of A_1 ($P_{11}, P_{12} \sim 0$), see Eq. 2.6 and, hence the fermion couplings ($g_u^{A_1}, g_d^{A_1}$) approach to almost negligible value ($\sim 10^{-5}$), and, hence the corresponding fermionic loop contribution in Eq. 3.6 are extremely suppressed. On the other hand, the presence of Higgsino composition in the chargino state yields a favorable coupling with A_1 via the singlet-Higgsino-Higgsino interaction (see the term proportional to λ in Eq. 3.9). Needless to say, that it is purely a typical NMSSM effect. Naturally, it is interesting to identify the region of the parameter space which offers a finite partial width of $A_1 \rightarrow \gamma\gamma$

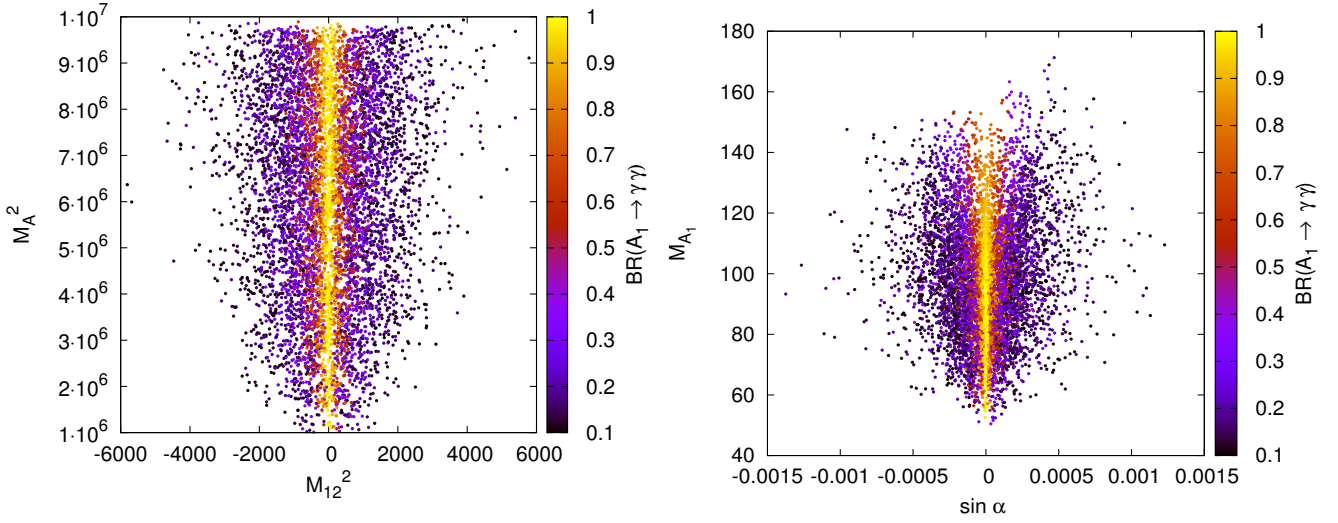


Figure 7: $\text{BR}(A_1 \rightarrow \gamma\gamma)$ in the $M_A^2 - M_{12}^2$ (left) and $\sin \alpha - M_{A_1}$ plane (right). The other parameters are varied for the range, as given in Eq.3.1. All energy unit are in GeV.

mode. We try to study it by examining the mixing of CP odd Higgs bosons states via the mass matrix, Eq. 3.2–3.3. Recall, that a very small value of $\sin \alpha$ leads a singlet dominated A_1 state resulting a suppression of its couplings with the fermions. Following the mass matrix, it can be realized very easily that the lighter CP odd state A_1 , can be a very much singlet like in the presence of negligible mixing between A and S states and, essentially it can happen due to either of the following two conditions:

1. $M_A^2 \gg M_S^2, M_{12}^2$ *i.e* the heavier state is too heavy and purely doublet like where as the lighter state is singlet, a decoupled type of scenario.
2. $M_{12}^2 = (A_\lambda - 2\kappa v_s) \sim 0$, *i.e*, a cancellation between two the terms in the off-diagonal element.

These two scenarios are illustrated in Fig.7, presenting the range of M_A^2 and M_{12}^2 (Eq.3.2, 3.3), corresponding to $\text{BR}(A_1 \rightarrow \gamma\gamma) \gtrsim 10\%$. In the left panel, we present the range of diagonal term M_A^2 and the off-diagonal element M_{12}^2 of the mass matrix M_p^2 , Eq. 3.2. As expected, for very low values of $M_{12}^2 (\sim 0)$ and corresponding to larger values of $M_A^2 \sim 10^6$, $\text{BR}(A_1 \rightarrow \gamma\gamma)$ appears to be ($\gtrsim 80\%$), and even for the case $0 < |M_{12}^2| \ll M_A^2$, it can be about 10-20%. It also indicates that the $\text{BR}(A_1 \rightarrow \gamma\gamma)$ becomes almost 100% for the scenario $M_{12}^2 \sim 0$, *i.e* $A_\lambda \sim 2\kappa v_s$. Moreover, we show the range of mixing angle in terms of $\sin \alpha$ and the mass of A_1 in Fig.7(right), corresponding to the range of M_{12}^2 and M_A^2 , as shown in the left panel of the same figure. It clearly confirms the smallness of the mixing angle responsible to yield a large $\text{BR}(A_1 \rightarrow \gamma\gamma)$

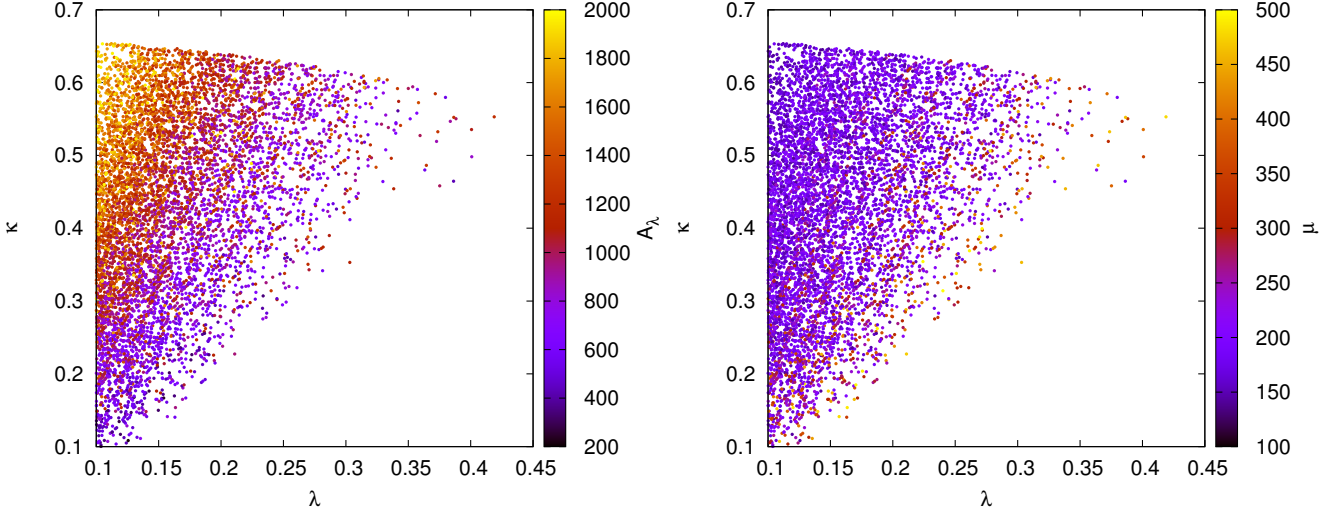


Figure 8: $BR(A_1 \rightarrow \gamma\gamma)(\geq 10\%)$ in the $\lambda - \kappa$ plane for the range of A_λ (left) and μ_{eff} (right). The other parameters are varied for the range, as given in Eq.3.1.

and it occurs for a wide range of M_{A_1} . Similarly, corresponding to the range of parameters as shown in Fig.7, for which $BR(A_1 \rightarrow \gamma\gamma) \gtrsim 10\%$, the relevant range of A_λ and μ_{eff} are shown in the $\lambda - \kappa$ plane in the left and right panel of Fig. 8 respectively. It is observed that a reasonable wide ranges of $\lambda(0.1 - 0.4)$ and $\kappa(0.1 - 0.65)$ can provide a large $BR(A_1 \rightarrow \gamma\gamma)$ for a larger range of A_λ and for a moderately large values of μ_{eff} . It is to be noted also that preferably Higgsino like lighter chargino i.e a smaller μ_{eff} as compared to M_2 , required in order to enhance the partial width of this channel.

Finally, based on the above observations about the parameter dependence of the production cross sections, $BR(\tilde{\chi}_2^0 \rightarrow \tilde{\chi}_1^0 A_1)$ and $BR(A_1 \rightarrow \gamma\gamma)$, we set up few benchmark points (BP) in order to present results. In summary, the preferred choices are, $\tilde{\chi}_1^0$ as a bino-Higgsino mixed state, $\tilde{\chi}_{2,3}^0$ and $\tilde{\chi}_1^\pm$ primarily Higgsino like, i.e $M_1 < \mu_{eff}$, but not with large gap between M_1 and μ_{eff} , and M_2 set to a larger value satisfying $M_2 > \mu_{eff}$. In Table 1, we show six BPs and presenting the corresponding parameters, masses of relevant particles and BRs. Notice that BP1-BP4 present comparatively lighter masses of chargino and neutralino states, whereas these are massive for BP5 and BP6. The values of M_{A_1} are chosen in such a way that the decay of the SM Higgs to a pair of A_1 is forbidden in order to make it compatible with recent SM Higgs boson results [58]. For all BPs, the lightest CP even Higgs boson, H_1 is SM-like. Although, both the $\tilde{\chi}_2^0$ and $\tilde{\chi}_3^0$ neutralino states are Higgsino like, but, more precisely, the coupling strength depends on the kind of Higgsino composition, either it is \tilde{H}_u or \tilde{H}_d (see Eq. 3.5) like. Notice that, for BP4, because of the higher mass of A_1 , the $A_1 \rightarrow Z\gamma$ also opens up and found

	BP1	BP2	BP3	BP4	BP5	BP6
λ	0.29	0.40	0.10	0.53	0.64	0.50
κ	0.37	0.45	0.20	0.39	0.36	0.48
$\tan \beta$	6.46	6.46	11.0	4.0	2.5	2.84
M_A	1722	340.7	1311.5	1262.4	1436.9	1655.8
A_κ	-4.97	-4.97	-3.9	-5.8	-6.5	-9.37
μ_{eff}	342.4	200.0	158.5	365.4	636.8	540.7
M_1	300	150.0	135.4	275.9	605.8	514.0
M_2	606.6	606.6	1000.0	9000	1857.4	1597.1
$M_{\tilde{\chi}_1^0}$	280.6	131.4	113.4	261.8	578.3	488.5
$M_{\tilde{\chi}_2^0}$	356.4	210.0	169.0	379.1	657.5	559.8
$M_{\tilde{\chi}_3^0}$	356.7	215.6	182.3	385.5	661.0	572.7
$M_{\tilde{\chi}_1^\pm}$	340.0	199.3	161.7	377.5	648.6	550.6
M_{A_1}	62	76	63.1	105.2	62.8	66.8
M_{H_1}	124	124	124	124	125	123
$BR(\chi_2^0 \rightarrow \tilde{\chi}_1^0 A_1)$	0.92	0.83	0.0	0.44	0.98	0.05
$BR(\chi_3^0 \rightarrow \tilde{\chi}_1^0 A_1)$	0.27	0.31	0.52	0.002	0.11	0.97
$BR(A_1 \rightarrow \gamma\gamma)$	0.79	0.91	0.98	0.87	0.97	0.97

Table 1: Parameters, masses, and BRs for six benchmark points.

to be its BR around $\sim 2\%$. This decay channel of A_1 can give rise to a spectacular signal with the final state $Z\gamma$ along with a lepton and \cancel{E}_T , when it is produced through the production mechanism, as shown in Eq.1.2.

4 Signal and Background

In this section we present the detection prospect of finding the signal $\gamma\gamma + \ell^\pm + \cancel{E}_T$ at the LHC with the center of mass energy, $\sqrt{S} = 13$ TeV, corresponding to a few integrated luminosity options. As mentioned in the previous section, the signal events appear from both the $\tilde{\chi}_1^\pm \tilde{\chi}_2^0$ and $\tilde{\chi}_1^\pm \tilde{\chi}_3^0$ production following the cascade decays, $\tilde{\chi}_{2,3}^0 \rightarrow \tilde{\chi}_1^0 A_1$, and $A_1 \rightarrow \gamma\gamma$ (Eq. 1.2). The lepton originates mainly from $\tilde{\chi}_1^\pm \rightarrow \ell^\pm \nu \tilde{\chi}_1^0$ decay and the missing transverse energy (\cancel{E}_T) arises due to the presence of massive LSPs, in addition to almost massless neutrinos. The dominant SM background contributions come from the following processes,

$$pp \rightarrow W\gamma, \quad Z\gamma, \quad W\gamma\gamma, \quad Z\gamma\gamma, \quad (4.1)$$

with the leptonic decays of W/Z . Note that in the first two cases, the second photon originates primarily from the initial state, radiated by incoming quarks. In addition, the another potential source of backgrounds are due to the faking of jets as photon in the process,

$$pp \rightarrow W\gamma j, \quad Z\gamma j, \quad (4.2)$$

and interestingly, it is found to be the dominant ones.

In our simulation we generate signal events using **PYTHIA6** [59] providing spectrum of SUSY particles and BR of various decay channels through SLHA file [60], obtained from **NMSSMTools** [54], corresponding to our chosen parameter space, as shown in Table 1. The background events with 2-body at the final state($W\gamma, Z\gamma$) are generated directly using **PYTHIA6**, while processes consisting 3-body are simulated using the Mad-Graph [61] and then **PYTHIA6** is used for showering. The generated events are stored in the standard HEP format (STDHEP) [62] to pass them through **Delphes3.2.0** [63] to take into account the detector effects. In our analysis we have used the default CMS card in Delphes, but results are also checked with ATLAS default card and not much differences are observed.

The objects in the final state such as, electron, photon and missing transverse energy are identified and reconstructed using Delphes based algorithms [63]. However, for the sake of completeness, we describe very briefly the object reconstruction techniques followed in the Delphes.

- **Lepton Selection:** The electrons are reconstructed using the information from the tracker and ECAL parameterizing the combined reconstruction efficiency as a function of the energy and pseudorapity. The muons are reconstructed using the predefined reconstruction efficiency and the final momentum is obtained by a Gaussian smearing of the initial 4-momentum vector. In our simulation, both the electrons and the muons are selected, imposing cuts on the transverse momenta (p_T^ℓ) and pseudo rapidity (η^ℓ) of lepton as,

$$p_T^\ell \geq 20 \text{ GeV}; \quad |\eta^\ell| \leq 2.5; \quad (l = e, \mu), \quad (4.3)$$

where η^ℓ restriction is due to the limited tracker coverage. The leptons are required to be isolated by demanding the total transverse energy $E_T^{ac}(\ell) \leq 20\%$ of the p_T^ℓ , where $E_T^{ac}(\ell)$ is the scalar sum of transverse energies of particles with minimum transverse momentum 0.5 GeV around the lepton direction within a cone size of $\Delta R = 0.5$.

- Photon Selection: The genuine photons and electrons that reach to the ECAL having no reconstructed tracks are considered as photons in the Delphes neglecting the conversions of photons into electron-positron pairs. In the present version of Delphes 3.2.0, the fake rate of photons are not simulated. In our simulation, we select photons subject to cuts,

$$p_T^\gamma > 20 \text{ GeV}; \quad |\eta^\gamma| < 2.4, \quad (4.4)$$

but excluding the η region, $1.44 < |\eta|^\gamma < 1.57$. The isolation of photon is ensured by measuring the sum of transverse momenta $E_T^{ac}(\gamma)$ of all particles around $\Delta R=0.5$ along the of the axis of the photon and transverse momentum more than 0.5 GeV. We consider photon is isolated if,

$$E_{AC}^T(\gamma) < 0.2 p_T^\gamma. \quad (4.5)$$

- Missing transverse energy: In the Delphes, the missing transverse energy is estimated from the transverse component of the total energy deposited in the detector, as defined,

$$\vec{\cancel{E}}_T = - \sum \vec{p}_T(i) \quad (4.6)$$

where i runs over all measured collection from the Detector. In the signal event \cancel{E}_T is expected to be harder as it appears due to the comparatively heavier object $\tilde{\chi}_1^0$, where as in the SM it is mainly due to the neutrinos. Hence, \cancel{E}_T may be a useful variable to isolate background events by a good fraction without affecting signal events too much. A cut,

$$\cancel{E}_T > 50 \text{ GeV}, \quad (4.7)$$

is applied in our simulation and observed that a substantial fraction ($\gtrsim 50\%$) of background events are rejected with a mild loss of signal events.

With a goal to separate out the signal from the background events, we investigate several kinematic variables. We notice that the p_T^γ are comparatively harder in the signal than the background events. This can be attributed to the fact that the photons in the signal events originate from A_1 decay, which is to some extent expected to be boosted as it is produced from heavier neutralino states. On the other hand, in the background process photons arise due to soft or hard emission accompanied with a W/Z boson and are not as boosted as in the signal events. Hence, we impose following

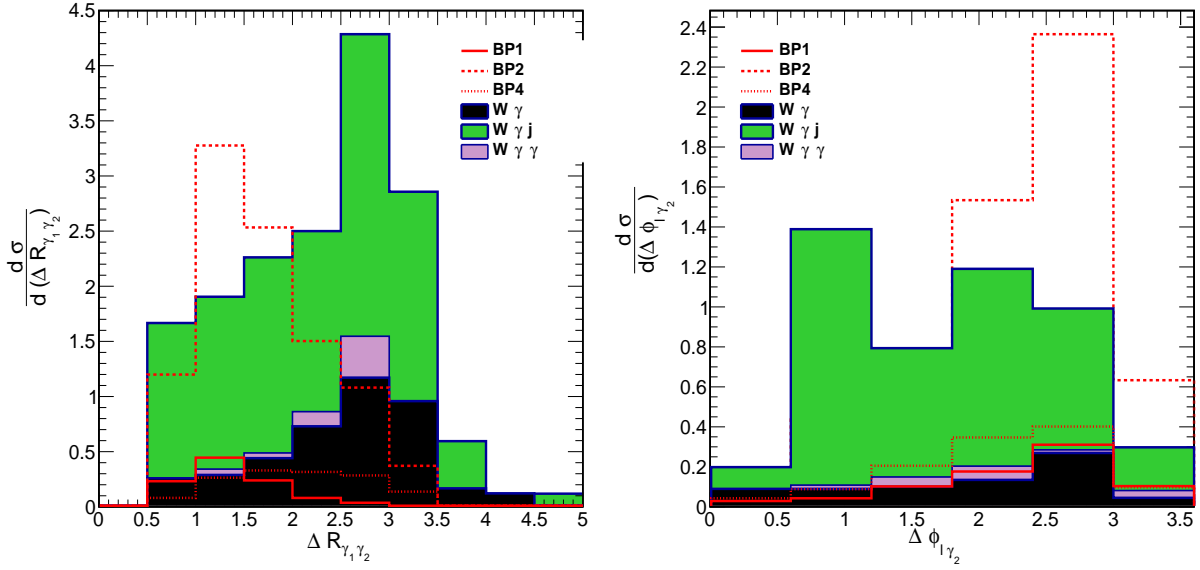


Figure 9: $\Delta R_{\gamma_1 \gamma_2}$ (left) and $\Delta \phi_{l \gamma_2}$ (right) distribution for both the signal and dominant backgrounds. These are subject to selection cuts, Eqs. 4.3, 4.7, 4.8.

hard cut on the leading (γ_1) photon and little mild on the sub-leading (γ_2) photon to eliminate background events,

$$p_T^{\gamma_1} > 40 \text{ GeV}; \quad p_T^{\gamma_2} > 20 \text{ GeV}. \quad (4.8)$$

Moreover, interestingly, we observed that the distribution of $\Delta R_{\gamma_1 \gamma_2}$, defined as,

$$\Delta R_{\gamma_1 \gamma_2} = \sqrt{(\eta_{\gamma_1} - \eta_{\gamma_2})^2 + (\phi_{\gamma_1} - \phi_{\gamma_2})^2}, \quad (4.9)$$

presents a characteristic feature for the signal events. Two photons in signal events originating from a comparatively massive A_1 are expected to be correlated and appear without much angular separation between them, unlike the background events, where these are not directly correlated and come out with a comparatively wider angular separation. This interesting feature is clearly demonstrated in the distribution of $\Delta R_{\gamma_1 \gamma_2}$, as shown in Figure 9 (left), for both the signal and dominant backgrounds, such as $W\gamma$, $W\gamma\gamma$, $W\gamma j$. Note that, $\Delta R_{\gamma_1 \gamma_2}$ distributions are subject to cuts given by Eqs. 4.3, 4.7, 4.8. It displays a clear difference, where the signal events are distributed in the lower region of $\Delta R_{\gamma_1 \gamma_2}$, where as the background events mostly appear towards the higher side. Evidently, this characteristic feature can be exploited to improve the purity of the signal events. Optimizing the selection of $\Delta R_{\gamma_1 \gamma_2}$, we require,

$$\Delta R_{\gamma_1 \gamma_2} \leq 2.0 \quad (4.10)$$

in our simulation and eliminate a good fraction of background events. Finally, to minimize the background contamination further, in particular due to the most dominant $W\gamma j$ process, we construct another observable, the difference in the azimuthal angle between the lepton and the sub-leading photon *i.e* $\Delta\phi_{\ell\gamma_2}$. In Fig. 9(right), we present the distribution of $\Delta\phi_{\ell\gamma_2}$ for both the signal and the dominant backgrounds($W\gamma$, $W\gamma j$, $W\gamma\gamma$). This distribution clearly shows a difference in behavior of the signal events which are distributed towards the higher values of $\Delta\phi_{\ell\gamma_2}$, while the dominant $W\gamma j$ background does not show any such pattern. Hence, a selection of $\Delta\phi_{\ell\gamma_2}$ as,

$$\Delta\phi_{\ell\gamma_2} > 1.5. \quad (4.11)$$

further suppresses the $W\gamma j$ background without much reduction of the signal size. Also note that in this selected region of $\Delta\phi_{\ell\gamma_2}$, only the signal contribution corresponding to the BP1 point is large, while for the other BPs, it is more or less at the same level as backgrounds. Implementing all selection cuts together in the simulation, we achieve a reasonable signal sensitivity as discussed in the next section.

5 Results

In Table 2, we present the summary of our simulation for both the signal and the SM backgrounds showing the number of events remaining after applying a given set of cuts. The results are shown for the signal corresponding to six BPs as shown in the Table 1. The third column presents the production cross sections and N_{ev} in the 4th column indicates the number of events simulated for each processes. A k-factor 1.3 is used for the signal cross section in order to take into account NLO effects [51]. The NLO cross sections for background processes are evaluated using **MadGraph aMC@NLO** [64] subject to $p_T^\gamma > 10 \text{ GeV}$ and $|\eta^\gamma| < 2.5$ for photons, where as $p_T^j > 20 \text{ GeV}$ and $|\eta^j| < 5$ are also used for accompanied jets at the generating level. Requirement of two hard photons and single lepton reduce the background contributions substantially by 3-5 orders of magnitude, where as the signal events decrease by about an order. The $\cancel{E}_T > 50 \text{ GeV}$ selection is very effective in suppressing backgrounds, in particular process accompanying with a Z -boson in which case there is no genuine source of \cancel{E}_T . The selection of $\Delta R_{\gamma_1\gamma_2}$ appears to be very useful, as discussed above, in eliminating backgrounds by 60-80% with a marginal reduction in signal events. Evidently, the dominant background contamination turn out to be due to the $W\gamma j$, which is about 65% of the total background contribution. Notably, the background processes associated with a Z boson are not contributing significantly, because of the requirement of single lepton and a strong \cancel{E}_T . The signal benchmark points BP2 and BP3, comparatively

	Process	$\sigma(\text{NLO})$	N_{ev}	$N_\gamma \geq 2$	$N_l = 1$	$\cancel{E}_T \geq 50$	$\Delta R_{\gamma_1 \gamma_2} \leq 2$	$\Delta \phi_{l \gamma_2} \geq 1.5$	$\sigma \times \epsilon$ (fb)
BP1	$\tilde{\chi}_2^0 \tilde{\chi}_1^\pm$	36.4 fb	0.3L	7124	886	569	502	426	0.38
	$\tilde{\chi}_3^0 \tilde{\chi}_1^\pm$	44.8 fb	0.3L	7006	879	587	519	431	0.14
BP2	$\tilde{\chi}_2^0 \tilde{\chi}_1^\pm$	335 fb	0.3L	9303	1140	590	415	346	2.9
	$\tilde{\chi}_3^0 \tilde{\chi}_1^\pm$	442 fb	0.3L	9593	1213	682	499	418	1.7
BP3	$\tilde{\chi}_3^0 \tilde{\chi}_1^\pm$	539 fb	0.3L	5755	589	312	270	240	2.2
BP4	$\tilde{\chi}_2^0 \tilde{\chi}_1^\pm$	61.1 fb	0.3L	14750	2555	1916	910	738	0.6
	$\tilde{\chi}_3^0 \tilde{\chi}_1^\pm$	43.9 fb	0.3L	14827	2447	1873	935	730	0.002
BP5	$\tilde{\chi}_2^0 \tilde{\chi}_1^\pm$	4.00 fb	0.3L	7798	1023	715	598	475	0.060
	$\tilde{\chi}_3^0 \tilde{\chi}_1^\pm$	1.80 fb	0.3L	8292	1111	809	694	540	0.003
BP6	$\tilde{\chi}_2^0 \tilde{\chi}_1^\pm$	8.80 fb	0.3L	7549	893	497	353	288	0.004
	$\tilde{\chi}_3^0 \tilde{\chi}_1^\pm$	4.90 fb	0.3L	9135	1132	813	634	517	0.080
Bkg.	$W\gamma$	215 pb	30M	15002	1117	272	65	47	0.33
	$Z\gamma$	103 pb	30M	14792	1506	52	12	10	0.03
	$W\gamma j$	125 pb	2.1M	2987	282	137	49	30	1.80
	$Z\gamma j$	45 pb	2.1M	2531	1203	27	10	6	0.13
	$W\gamma\gamma$	407 fb	0.5L	6011	760	260	66	47	0.40
	$Z\gamma\gamma$	257 fb	0.5L	5312	233	12	7	4	0.02

Table 2: Event summary for the signal and backgrounds(Bkg) subject to a set of cuts. The last column presents the cross section after multiplying the acceptance efficiency including BRs.

with lower masses of $\tilde{\chi}_1^\pm$ and $\tilde{\chi}_2^0$ yield larger event rates, primarily due to the large production cross sections. The last columns shows the cross sections normalized by the selection efficiency due to set selections for each processes and parameters. space.

In Table 3, we show the sensitivity of the signal presenting the significances (S/\sqrt{B}) for three integrated luminosity options 100, 300 and 1000 fb^{-1} . The total background cross section is estimated to be about 2.74 fb. In this table the second row presents the signal cross section corresponding to each BPs. The significances are quite encouraging for the lower masses ($\leq 400 \text{ GeV}$) of $\tilde{\chi}_1^\pm$, $\tilde{\chi}_{2,3}^0$ and for $A_1 \sim 60$ -100 GeV, even for low integrated luminosity $\mathcal{L} = 100 \text{ fb}^{-1}$. However, for the higher range of masses (BP5 and BP6), the sensitivity is very poor due to tiny production cross sections. We emphasize again that in order to obtain a sizeable signal rate, the chosen parameter space are happen to be a compressed scenario. In case of the scenario represented by BP4, where $M_1 < \mu_{eff}$, $\tilde{\chi}_{2,3}^0$ decays to relatively massive of A_1 .

Remarkably, this signal is observable for some of the BPs corresponding to comparatively lower masses of $\tilde{\chi}_{2,3}^0$ and $\tilde{\chi}_1^\pm$ for the 300 fb^{-1} luminosity option and very robust

Process	BP1	BP2	BP3	BP4	BP5	BP6
$\sigma \times \epsilon$ (fb)	0.52	4.6	2.2	0.6	0.063	0.084
\mathcal{L} (fb $^{-1}$)	S/\sqrt{B}					
100	3.1	28.1	13.3	3.5	0.40	0.50
300	5.4	48.7	23.9	6.0	0.67	0.88
1000	9.8	89.0	42.0	11.0	1.22	1.60

Table 3: The signal cross sections after multiplying the acceptance efficiency including BRs(2nd row) and significance (S/\sqrt{B}) for three integrated luminosity options 100, 300 and 1000 fb $^{-1}$. The total background cross-section is 2.74 fb.

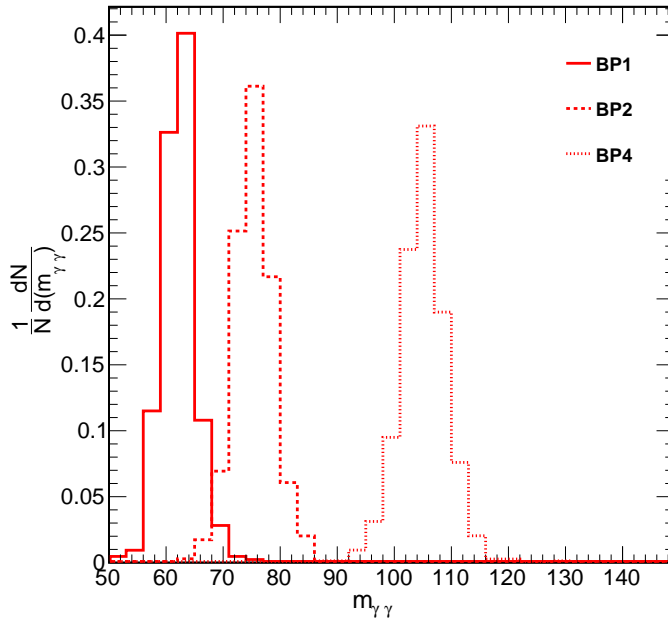


Figure 10: Two photon invariant mass for three signal BPs normalizing to unity.

for high luminosity option 1000 fb $^{-1}$. Furthermore, it is worth to mention here that in analogy with the SM Higgs searches, in this study also, the di-photon invariant mass is expected to show a clear peak at the mass of A_1 . In Fig.10, we show the distribution of reconstructed $m_{\gamma\gamma}$ subject to all cuts as listed in Table.2. Because of the low statistics of background events after selection, those are not shown in this figure. Perhaps, the level of background contamination can be reduced further by fitting the signal peak leading an enhancement of signal sensitivity.

6 Summary

In the NMSSM, one of the non SM-like Higgs boson, particularly lightest pseudoscalar A_1 , which is mostly singlet like, can decay to di-photon channel via Higgsino like chargino loop with a substantial BR. We identify the region of the parameter space corresponding to $\text{BR}(\tilde{\chi}_{2,3}^0 \rightarrow \tilde{\chi}_1^0 A_1)$ and $\text{BR}(A_1 \rightarrow \gamma\gamma) \geq$, both at the level of 10% or more and present the potential ranges of λ, κ along with μ_{eff}, A_λ . We investigate the sensitivity of the signal $\ell + \gamma\gamma + \cancel{E}_T$ producing A_1 through the chargino-neutralino associated production as shown in Eq.1.2. The possible contamination due to the SM backgrounds are also estimated and $W\gamma j$ is found to be the dominant one, where jet fakes as a photon. Performing a detail simulation of the signal and the background processes including detector effects using Delphes, we predict the signal sensitivity for few benchmark points and for a given integrated luminosity options for the LHC Run 2 experiments. Our simulation shows that this signal is observable marginally for $100 fb^{-1}$ integrated luminosity. However, for larger integrated luminosity option, this signal is very robust and $S/\sqrt{B} \gg 5\sigma$ sensitivity can be achieved for the $m_{\tilde{\chi}_{2,3}^0}, m_{\tilde{\chi}_1^\pm} \sim 400$ GeV and $M_{A_1} \sim 70$ GeV, where as it severely degrades for higher masses ~ 600 GeV due to the heavily suppressed cross section. The reconstructed di-photon invariant mass is expected to show a clear visible narrow peak around the mass of A_1 , which can be exploited to suppress backgrounds further to improve the signal sensitivity. Hence, room for a possible more improvements of signal to background ratio exist, which is not explored in the current study. We reiterate here that two photons BR of Higgs boson is heavily suppressed in the SM and as well as in the MSSM. In this context, we emphasize again very strongly that this diphoton decay mode of A_1 can be used as a powerful tool to distinguish the NMSSM from the other SUSY models.

7 Acknowledgment

JK would like to thank Bibhu P. Mahakud, Jyoti Ranjan Beuria and Michael Paraskevas for useful discussions. The authors are also thankful to Saurabh Nioygi for participating in this project in the beginning.

References

- [1] **ATLAS** Collaboration, G. Aad *et al.*, “Observation of a new particle in the search for the Standard Model Higgs boson with the ATLAS detector at the LHC,” *Phys. Lett. B* **716** (2012) 1–29, [arXiv:1207.7214 \[hep-ex\]](#).

- [2] **CMS** Collaboration, S. Chatrchyan *et al.*, “Observation of a new boson at a mass of 125 GeV with the CMS experiment at the LHC,” *Phys. Lett.* **B716** (2012) 30–61, [arXiv:1207.7235 \[hep-ex\]](#).
- [3] L. J. Hall, D. Pinner, and J. T. Ruderman, “A Natural SUSY Higgs Near 126 GeV,” *JHEP* **04** (2012) 131, [arXiv:1112.2703 \[hep-ph\]](#).
- [4] A. Arbey, M. Battaglia, A. Djouadi, F. Mahmoudi, and J. Quevillon, “Implications of a 125 GeV Higgs for supersymmetric models,” *Phys. Lett.* **B708** (2012) 162–169, [arXiv:1112.3028 \[hep-ph\]](#).
- [5] J. E. Kim and H. P. Nilles, “The mu Problem and the Strong CP Problem,” *Phys. Lett.* **B138** (1984) 150–154.
- [6] P. Fayet, “Supergauge Invariant Extension of the Higgs Mechanism and a Model for the electron and Its Neutrino,” *Nucl. Phys.* **B90** (1975) 104–124.
- [7] J. R. Ellis, J. F. Gunion, H. E. Haber, L. Roszkowski, and F. Zwirner, “Higgs Bosons in a Nonminimal Supersymmetric Model,” *Phys. Rev.* **D39** (1989) 844.
- [8] M. Drees, “Supersymmetric Models with Extended Higgs Sector,” *Int. J. Mod. Phys.* **A4** (1989) 3635.
- [9] U. Ellwanger, C. Hugonie, and A. M. Teixeira, “The Next-to-Minimal Supersymmetric Standard Model,” *Phys. Rept.* **496** (2010) 1–77, [arXiv:0910.1785 \[hep-ph\]](#).
- [10] D. J. Miller, R. Nevzorov, and P. M. Zerwas, “The Higgs sector of the next-to-minimal supersymmetric standard model,” *Nucl. Phys.* **B681** (2004) 3–30, [arXiv:hep-ph/0304049 \[hep-ph\]](#).
- [11] Z. Kang, J. Li, and T. Li, “On Naturalness of the MSSM and NMSSM,” *JHEP* **11** (2012) 024, [arXiv:1201.5305 \[hep-ph\]](#).
- [12] J. Cao, F. Ding, C. Han, J. M. Yang, and J. Zhu, “A light Higgs scalar in the NMSSM confronted with the latest LHC Higgs data,” *JHEP* **11** (2013) 018, [arXiv:1309.4939 \[hep-ph\]](#).
- [13] D. Albornoz Vasquez, G. Belanger, C. Boehm, J. Da Silva, P. Richardson, and C. Wymant, “The 125 GeV Higgs in the NMSSM in light of LHC results and astrophysics constraints,” *Phys. Rev.* **D86** (2012) 035023, [arXiv:1203.3446 \[hep-ph\]](#).

- [14] S. F. King, M. Muhlleitner, and R. Nevzorov, “NMSSM Higgs Benchmarks Near 125 GeV,” *Nucl. Phys.* **B860** (2012) 207–244, [arXiv:1201.2671 \[hep-ph\]](#).
- [15] S. Heinemeyer, O. Stal, and G. Weiglein, “Interpreting the LHC Higgs Search Results in the MSSM,” *Phys. Lett.* **B710** (2012) 201–206, [arXiv:1112.3026 \[hep-ph\]](#).
- [16] F. Domingo and G. Weiglein, “NMSSM interpretations of the observed Higgs signal,” *JHEP* **04** (2016) 095, [arXiv:1509.07283 \[hep-ph\]](#).
- [17] A. Djouadi *et al.*, “Benchmark scenarios for the NMSSM,” *JHEP* **07** (2008) 002, [arXiv:0801.4321 \[hep-ph\]](#).
- [18] S. F. King, M. Mhlleitner, R. Nevzorov, and K. Walz, “Natural NMSSM Higgs Bosons,” *Nucl. Phys.* **B870** (2013) 323–352, [arXiv:1211.5074 \[hep-ph\]](#).
- [19] N. D. Christensen, T. Han, Z. Liu, and S. Su, “Low-Mass Higgs Bosons in the NMSSM and Their LHC Implications,” *JHEP* **08** (2013) 019, [arXiv:1303.2113 \[hep-ph\]](#).
- [20] J. Kumar and M. Paraskevas, “Distinguishing between MSSM and NMSSM through $\Delta F = 2$ processes,” [arXiv:1608.08794 \[hep-ph\]](#).
- [21] M. Guchait and J. Kumar, “Light Higgs Bosons in NMSSM at the LHC,” *Int. J. Mod. Phys.* **A31** no. 12, (2016) 1650069, [arXiv:1509.02452 \[hep-ph\]](#).
- [22] J. F. Gunion, Y. Jiang, and S. Kraml, “The Constrained NMSSM and Higgs near 125 GeV,” *Phys. Lett.* **B710** (2012) 454–459, [arXiv:1201.0982 \[hep-ph\]](#).
- [23] U. Ellwanger and C. Hugonie, “Higgs bosons near 125 GeV in the NMSSM with constraints at the GUT scale,” *Adv. High Energy Phys.* **2012** (2012) 625389, [arXiv:1203.5048 \[hep-ph\]](#).
- [24] M. Badziak, M. Olechowski, and S. Pokorski, “New Regions in the NMSSM with a 125 GeV Higgs,” *JHEP* **06** (2013) 043, [arXiv:1304.5437 \[hep-ph\]](#).
- [25] **CMS** Collaboration, S. Chatrchyan *et al.*, “Search for a light pseudoscalar Higgs boson in the dimuon decay channel in pp collisions at $\sqrt{s} = 7$ TeV,” *Phys. Rev. Lett.* **109** (2012) 121801, [arXiv:1206.6326 \[hep-ex\]](#).
- [26] **CMS** Collaboration, V. Khachatryan *et al.*, “Search for a low-mass pseudoscalar Higgs boson produced in association with a $b\bar{b}$ pair in pp collisions at $\sqrt{s} = 8$ TeV,” *Phys. Lett.* **B758** (2016) 296–320, [arXiv:1511.03610 \[hep-ex\]](#).

- [27] **ATLAS** Collaboration, G. Aad *et al.*, “Search for Higgs bosons decaying to aa in the $\mu\mu\tau\tau$ final state in pp collisions at $\sqrt{s} = 8$ TeV with the ATLAS experiment,” *Phys. Rev.* **D92** no. 5, (2015) 052002, [arXiv:1505.01609 \[hep-ex\]](#).
- [28] **ATLAS** Collaboration, G. Aad *et al.*, “Search for new phenomena in events with at least three photons collected in pp collisions at $\sqrt{s} = 8$ TeV with the ATLAS detector,” *Eur. Phys. J.* **C76** no. 4, (2016) 210, [arXiv:1509.05051 \[hep-ex\]](#).
- [29] U. Ellwanger, J. F. Gunion, C. Hugonie, and S. Moretti, “NMSSM Higgs discovery at the LHC,” in *Physics at TeV colliders. Proceedings, Workshop, Les Houches, France, May 26-June 3, 2003*. 2004. [arXiv:hep-ph/0401228 \[hep-ph\]](#).
- [30] U. Ellwanger, “Higgs Bosons in the Next-to-Minimal Supersymmetric Standard Model at the LHC,” *Eur. Phys. J.* **C71** (2011) 1782, [arXiv:1108.0157 \[hep-ph\]](#).
- [31] S. F. King, M. Mhleitner, R. Nevzorov, and K. Walz, “Discovery Prospects for NMSSM Higgs Bosons at the High-Energy Large Hadron Collider,” *Phys. Rev.* **D90** no. 9, (2014) 095014, [arXiv:1408.1120 \[hep-ph\]](#).
- [32] F. Mahmoudi, J. Rathsmann, O. Stal, and L. Zeune, “Light Higgs bosons in phenomenological NMSSM,” *Eur. Phys. J.* **C71** (2011) 1608, [arXiv:1012.4490 \[hep-ph\]](#).
- [33] N.-E. Bomark, S. Moretti, S. Munir, and L. Roszkowski, “A light NMSSM pseudoscalar Higgs boson at the LHC redux,” *JHEP* **02** (2015) 044, [arXiv:1409.8393 \[hep-ph\]](#).
- [34] A. Belyaev, S. Hesselbach, S. Lehti, S. Moretti, A. Nikitenko, and C. H. Shepherd-Themistocleous, “The Scope of the 4 tau Channel in Higgs-strahlung and Vector Boson Fusion for the NMSSM No-Lose Theorem at the LHC,” [arXiv:0805.3505 \[hep-ph\]](#).
- [35] A. Belyaev, J. Pivarski, A. Safonov, S. Senkin, and A. Tatarinov, “LHC discovery potential of the lightest NMSSM Higgs in the $h1 \rightarrow a1 a1 \rightarrow 4$ muons channel,” *Phys. Rev.* **D81** (2010) 075021, [arXiv:1002.1956 \[hep-ph\]](#).
- [36] M. M. Almarashi and S. Moretti, “Muon Signals of Very Light CP-odd Higgs states of the NMSSM at the LHC,” *Phys. Rev.* **D83** (2011) 035023, [arXiv:1101.1137 \[hep-ph\]](#).

- [37] D. G. Cerdeno, P. Ghosh, and C. B. Park, “Probing the two light Higgs scenario in the NMSSM with a low-mass pseudoscalar,” *JHEP* **06** (2013) 031, [arXiv:1301.1325 \[hep-ph\]](#).
- [38] D. Curtin, R. Essig, and Y.-M. Zhong, “Uncovering light scalars with exotic Higgs decays to $b\bar{b}\mu^+\mu^-$,” *JHEP* **06** (2015) 025, [arXiv:1412.4779 \[hep-ph\]](#).
- [39] N.-E. Bomark, S. Moretti, and L. Roszkowski, “Detection prospects of light NMSSM Higgs pseudoscalar via cascades of heavier scalars from vector boson fusion and Higgs-strahlung,” *J. Phys.* **G43** no. 10, (2016) 105003, [arXiv:1503.04228 \[hep-ph\]](#).
- [40] A. Arhrib, K. Cheung, T.-J. Hou, and K.-W. Song, “Associated production of a light pseudoscalar Higgs boson with a chargino pair in the NMSSM,” *JHEP* **03** (2007) 073, [arXiv:hep-ph/0606114 \[hep-ph\]](#).
- [41] R. Dermisek and J. F. Gunion, “The NMSSM Solution to the Fine-Tuning Problem, Precision Electroweak Constraints and the Largest LEP Higgs Event Excess,” *Phys. Rev.* **D76** (2007) 095006, [arXiv:0705.4387 \[hep-ph\]](#).
- [42] J. E. Kim, H. P. Nilles, and M.-S. Seo, “Singlet Superfield Extension of the Minimal Supersymmetric Standard model with Peccei-Quinn symmetry and a Light Pseudoscalar Higgs Boson at the LHC,” *Mod. Phys. Lett.* **A27** (2012) 1250166, [arXiv:1201.6547 \[hep-ph\]](#).
- [43] U. Ellwanger and M. Rodriguez-Vazquez, “Discovery Prospects of a Light Scalar in the NMSSM,” *JHEP* **02** (2016) 096, [arXiv:1512.04281 \[hep-ph\]](#).
- [44] S. Moretti and S. Munir, “Di-photon Higgs signals at the LHC in the next-to-minimal supersymmetric standard model,” *Eur. Phys. J.* **C47** (2006) 791–803, [arXiv:hep-ph/0603085 \[hep-ph\]](#).
- [45] D. Ghosh, M. Guchait, and D. Sengupta, “Higgs Signal in Chargino-Neutralino Production at the LHC,” *Eur. Phys. J.* **C72** (2012) 2141, [arXiv:1202.4937 \[hep-ph\]](#).
- [46] D. G. Cerdezo, P. Ghosh, C. B. Park, and M. Peir, “Collider signatures of a light NMSSM pseudoscalar in neutralino decays in the light of LHC results,” *JHEP* **02** (2014) 048, [arXiv:1307.7601 \[hep-ph\]](#).
- [47] M. Guchait, “Exact solution of the neutralino mass matrix,” *Z. Phys.* **C57** (1993) 157–164. [Erratum: *Z. Phys.* **C61**, 178(1994)].

- [48] S. Y. Choi, J. Kalinowski, G. A. Moortgat-Pick, and P. M. Zerwas, “Analysis of the neutralino system in supersymmetric theories,” *Eur. Phys. J.* **C22** (2001) 563–579, [arXiv:hep-ph/0108117 \[hep-ph\]](#). [Addendum: *Eur. Phys. J.* **C23**, 769(2002)].
- [49] P. N. Pandita, “Neutralino mass matrix in the nonminimal supersymmetric Standard model,” *Z. Phys.* **C63** (1994) 659–671.
- [50] S. Y. Choi, D. J. Miller, and P. M. Zerwas, “The Neutralino sector of the next-to-minimal supersymmetric standard model,” *Nucl. Phys.* **B711** (2005) 83–111, [arXiv:hep-ph/0407209 \[hep-ph\]](#).
- [51] W. Beenakker, M. Klasen, M. Kramer, T. Plehn, M. Spira, and P. M. Zerwas, “The Production of charginos / neutralinos and sleptons at hadron colliders,” *Phys. Rev. Lett.* **83** (1999) 3780–3783, [arXiv:hep-ph/9906298 \[hep-ph\]](#). [Erratum: *Phys. Rev. Lett.* **100**, 029901(2008)].
- [52] H.-L. Lai, M. Guzzi, J. Huston, Z. Li, P. M. Nadolsky, J. Pumplin, and C. P. Yuan, “New parton distributions for collider physics,” *Phys. Rev.* **D82** (2010) 074024, [arXiv:1007.2241 \[hep-ph\]](#).
- [53] W. Beenakker, R. Hopker, and M. Spira, “PROSPINO: A Program for the production of supersymmetric particles in next-to-leading order QCD,” [arXiv:hep-ph/9611232 \[hep-ph\]](#).
- [54] U. Ellwanger, J. F. Gunion, and C. Hugonie, “NMHDECAY: A Fortran code for the Higgs masses, couplings and decay widths in the NMSSM,” *JHEP* **02** (2005) 066, [arXiv:hep-ph/0406215 \[hep-ph\]](#).
- [55] S. Munir, L. Roszkowski, and S. Trojanowski, “Simultaneous enhancement in $\gamma\gamma$, $b\bar{b}$ and $\tau^+\tau^-$ rates in the NMSSM with nearly degenerate scalar and pseudoscalar Higgs bosons,” *Phys. Rev.* **D88** no. 5, (2013) 055017, [arXiv:1305.0591 \[hep-ph\]](#).
- [56] M. Spira, A. Djouadi, D. Graudenz, and P. M. Zerwas, “Higgs boson production at the LHC,” *Nucl. Phys.* **B453** (1995) 17–82, [arXiv:hep-ph/9504378 \[hep-ph\]](#).
- [57] M. Spira, “QCD effects in Higgs physics,” *Fortsch. Phys.* **46** (1998) 203–284, [arXiv:hep-ph/9705337 \[hep-ph\]](#).

- [58] **ATLAS, CMS** Collaboration, G. Aad *et al.*, “Measurements of the Higgs boson production and decay rates and constraints on its couplings from a combined ATLAS and CMS analysis of the LHC pp collision data at $\sqrt{s} = 7$ and 8 TeV,” [arXiv:1606.02266](#) [[hep-ex](#)].
- [59] T. Sjostrand, S. Mrenna, and P. Z. Skands, “PYTHIA 6.4 Physics and Manual,” *JHEP* **05** (2006) 026, [arXiv:hep-ph/0603175](#) [[hep-ph](#)].
- [60] P. Z. Skands *et al.*, “SUSY Les Houches accord: Interfacing SUSY spectrum calculators, decay packages, and event generators,” *JHEP* **07** (2004) 036, [arXiv:hep-ph/0311123](#) [[hep-ph](#)].
- [61] **ATLAS** Collaboration, G. Aad *et al.*, “Search for direct pair production of a chargino and a neutralino decaying to the 125 GeV Higgs boson in $\sqrt{s} = 8$ TeV pp collisions with the ATLAS detector,” *Eur. Phys. J.* **C75** no. 5, (2015) 208, [arXiv:1501.07110](#) [[hep-ex](#)].
- [62] P. L. L. Garren, “StdHep User Manual,”.
- [63] **DELPHES 3** Collaboration, J. de Favereau, C. Delaere, P. Demin, A. Giammanco, V. Lematre, A. Mertens, and M. Selvaggi, “DELPHES 3, A modular framework for fast simulation of a generic collider experiment,” *JHEP* **02** (2014) 057, [arXiv:1307.6346](#) [[hep-ex](#)].
- [64] J. Alwall, R. Frederix, S. Frixione, V. Hirschi, F. Maltoni, O. Mattelaer, H. S. Shao, T. Stelzer, P. Torrielli, and M. Zaro, “The automated computation of tree-level and next-to-leading order differential cross sections, and their matching to parton shower simulations,” *JHEP* **07** (2014) 079, [arXiv:1405.0301](#) [[hep-ph](#)].